International Journal of Nanomedicine

Dovepress
open access to scientific and medical research

Open Access Full Text Article

ORIGINAL RESEARCH

Effective Attenuation of Arteriosclerosis Following Lymphatic-Targeted Delivery of Hyaluronic Acid-Decorated Rapamycin Liposomes

Xiaojia Liu[1,2], Caiyan Lin[1], Wenfei Zhong[1], Zhongwen Yuan[1], Pengke Yan[1], Shixia Guan[2]

[1]Department of Pharmacy, Biomedicine Research Center, Guangdong Provincial Key Laboratory of Major Obstetric Diseases, Guangdong Provincial Clinical Research Center for Obstetrics and Gynecology, The Third Affiliated Hospital of Guangzhou Medical University, Guangzhou, People's Republic of China; [2]School of Pharmaceutical Sciences, Guangzhou University of Chinese Medicine, Guangzhou, People's Republic of China

Correspondence: Pengke Yan; Shixia Guan, Email gysyypk@126.com; drguan@gzucm.edu.cn

Background: The activation of lymphatic vessel function is the crux to resolving atherosclerosis (AS), a chronic inflammatory disease. Rapamycin (RAPA) recently has attracted considerable attention as a potent drug to induce atherosclerotic plaque attenuation. The objective of this work was to develop a ligand-decorated, RAPA-loaded liposome for lymphatic-targeted delivery of drugs to improve abnormal lymphatic structure and function, resulting in highly effective regression of atherosclerotic plaques.

Methods: Hyaluronic acid-decorated, RAPA-loaded liposomes (HA-RL) were fabricated by emulsion-solvent evaporation. The average size, zeta potential, entrapment efficiency were characterized, and the stability and drug release in vitro were investigated. Furthermore, the in vitro and in vivo lymphatic targeting ability were evaluated on lymphatic endothelial cells and $LDLR^{-/-}$ mice, and the efficiency of this nano-system in inducing the attenuation of atherosclerotic plaques was confirmed.

Results: HA-RL had a size of 100 nm, over 90% drug encapsulation efficiency, the storage stability was distinguished, demonstrating a slow release from the lipid nano-carriers. The mean retention time (MRT) and elimination half-life ($t_{1/2\beta}$) achieved from HA-RL were 100.27±73.08 h and 70.74±50.80 h, respectively. HA-RL acquired the most prominent efficacy of lymphatic-targeted delivery and atherosclerotic plaques attenuation, implying the successful implementation of this novel drug delivery system in vivo.

Conclusion: HA-RL exhibited the most appreciable lymphatic targeting ability and best atherosclerotic plaques attenuation efficiency, opening a new paradigm and promising perspective for the treatment of arteriosclerosis.

Keywords: rapamycin, hyaluronic acid, lymphatic targeting, arteriosclerosis, liposomes

Introduction

Cardiovascular disease remains a major cause of morbidity and mortality worldwide.[1] Pathologically, the dominating etiology involves atherosclerosis, a chronic inflammatory disease characterized by the formation of lipid plaques in the intima of arteries, which can lead to life-threatening cardiovascular diseases such as coronary heart disease, myocardial infarction, stroke, and so on.[2,3] Immunosuppression therapy represents an attractive option.[4] In addition, there is increasing evidence that autophagy occurs in advanced atherosclerotic plaques.[5] Selectively activating autophagic death of macrophages could stabilize the fragile and ruptured lesions.[6,7] These findings strongly indicate that multi-active therapeutic agents are favorable for the inhibition of atherosclerosis progression.

Many antilipemic or antiplatelet agents are designed to prevent the later consequences of atherosclerosis, but not the process of lesion formation and progression. Rapamycin (RAPA), also known as sirolimus, an effective immunosuppressant that inhibits the mammalian target of the rapamycin (mTOR) pathway, has been used clinically for transplantation.[8] Given its anti-inflammatory, anti-proliferation, anti-migration, and autophagy activating properties, RAPA may have potential as an anti-atherosclerotic.[9] RAPA is able to inhibit growth factor-driven smooth muscle cell (SMC) proliferation, and prevent monocyte recruitment, lipid accumulation in macrophages and SMC, as well as being autophagy stimulating.[10–12] Additionally, it has been shown that RAPA can inhibit inflammatory immune responses, and

Received: 23 March 2023
Accepted: 10 June 2023
Published: 2 August 2023

modulate and stabilize atherosclerotic plaques.[13–15] Nevertheless, current oral RAPA delivery usually leads to significant fluctuations in plasma concentration, severe side effects, and elevated plasma triglyceride (TG) and low-density lipoprotein (LDL) levels.[16] In addition, high-dose RAPA stimulation can inhibit both mTOR complex 1 (mTORC1) and mTORC2 signaling pathways[17–19], while mTORC2 has multiple beneficial functions such as anti-inflammation, promoting endothelial cell survival and migration, and regulating Rit-mediated oxidative stress resistance.[20–22] However, considering that atherosclerosis is a chronic inflammatory disease and requires intervention in the long term, sustained delivery of RAPA with low doses is highly desirable for effective atherosclerosis therapy without obvious side effects.[22]

Nanomedicine has been deemed to be a tactic to manage cardiovascular-related diseases, and is also used for diagnosis and treatment by site-specific delivery.[23–29] Moreover, a nanocarrier drug delivery system (NDDS), as a potent means to optimize drug efficacy, has become an attractive focus in pharmaceutical research. Liposomes, which are multifunctional vesicles with a phospholipid bilayer structure, have been widely used in the delivery of therapeutic and diagnostic reagents, which benefit from their simple structure and specific targeting ability, especially the function of controlled release. They also have high biocompatibility and inherent lymphatic targeting properties, and show low toxicity and immunogenicity. However, one drawback of orthodox nanodelivery systems is the lack of targeted delivery at specific sites. One of the vital mechanisms for their limited targeting is that the phagocytic system will recognize nanoparticles as foreign, leading to rapid clearance.[30] Therefore, achieving a long half-life in blood circulation and site-specific targeting by engineering nanoparticles with ligands is highly desired. Surface-modified liposomes with ligands have also been proved to enhance lymph node accumulation by promoting specific receptor-ligand identification.[31] It has been reported that PEG-modified liposomes might enhance lymphatic drainage by increasing steric stabilization.[31,32] Hyaluronic acid, a negatively charged acidic mucopolysaccharide, has been applied to the surface of nanocarriers as an alternative to PEG, where a hydrated layer can be formed. The spatial stabilization and hydrophilicity of HA formation could prolong the residence time in vivo and reduce the non-specific delivery of nanoparticles.[33–35]

Studies have confirmed that atherosclerosis is a chronic inflammatory disease, and activation of lymphatic vessels has been shown to be the crux to resolving chronic inflammation.[36–40] Moreover, numerous hyperplastic lymphatic vessels and smooth muscle cells have been found around atherosclerotic vessels. It is reported that lymphatic vessels are not only involved in the initiation and regression of arterial inflammation, but also play a vital role in the reversal of cholesterol transport (expulsion of infiltrated glia and macromolecules from the arterial wall).[41–44] Lymphatic vessels have also been proved to be effective delivery channels for immunomodulators. Relevant studies have shown that HA has a high affinity with the surface receptors of lymph endothelial cells (lymphatic vessel endothelial hyaluronan receptor 1, LYVE-1).[38,45,46] In addition, HA also interacts with HARE (Stabilin-2) and CD44 receptors, as well as being associated with other proteins, including intracellular adhesion factors and related binding proteins.[47] Therefore, construction of nanoparticles responsive to these specific proteins may create an effective pathway for lymph-specific delivery. We hypothesized that reducing the proliferation of lymphatic vessels and smooth muscle cells by lymphatic targeted delivery of RAPA might be efficacious in attenuating atherosclerotic plaques.

A major goal of this work was to developed a lymphatic targeted nanoliposomes delivery system for atherosclerosis therapy (Figure 1). Rapamycin was loaded in liposomes as a model drug. This work aims at: (1) Fabricating hyaluronic acid-decorated liposomes via an emulsion-solvent evaporation method and studying physicochemical characterizations; (2) Investigating in vitro release behavior, pharmacokinetics, and biodistribution in vivo; (3) Studying the lymphatic targeting efficiency by near-infrared fluorescence imaging and laser confocal scanning microscopy; (4) Establishing an atherosclerosis model in $LDLR^{-/-}$mice and investigating the effects of different RAPA formulations on atherosclerotic plaques.

Materials and Methods

Materials and Animals

Rapamycin, phospholipid and sodium cholesterol sulfate were purchased from Avito Biotech Co., Ltd (Shanghai, China). All the other solvents and reagents used were of analytical grade (Supplementary Material Section S.1. Materials). Lymphatic endothelial cell (LECS) were supplied from ATCC (Manassas, VA, USA) (Supplementary Material Section S. 2. Cell Culture).

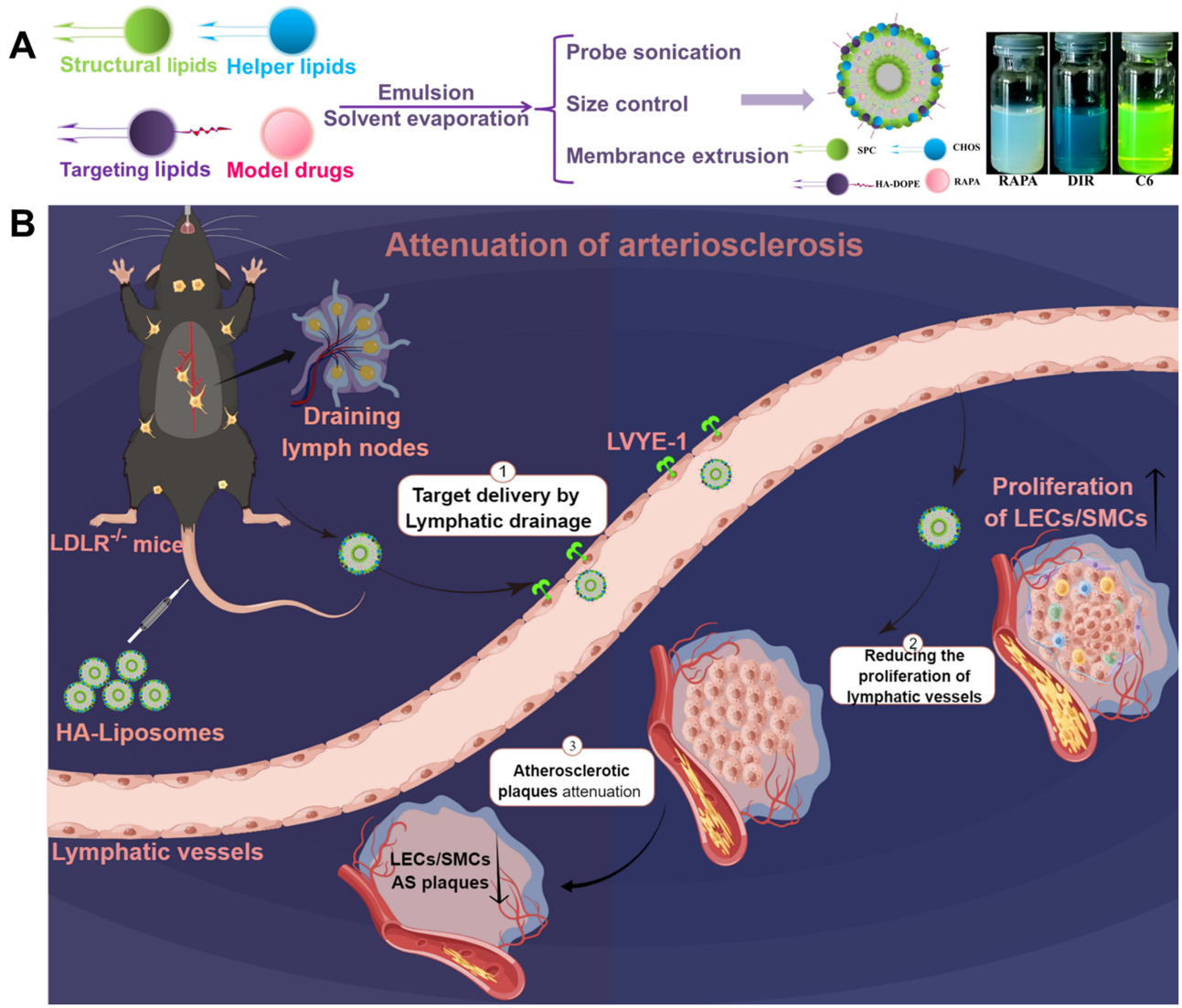

Figure 1 Illustrations displaying the fabrication of hyaluronic acid-decorated rapamycin liposomes (**A**), the lymphatic target delivery of liposomes and the regression of atherosclerotic plaques (**B**).

Sprague-Dawley rats (220–250 g) were supplied by the Animal Experimental Center of Guangzhou University of Chinese Medicine. Male LDLR$^{-/-}$ mice at 8 weeks of age were supplied by the third Affiliated Hospital of Guangzhou Medical University. All animals were acclimated and maintained in animal facilities with temperatures of 21–27°C, relative humidity of 50–60%, and a light/dark cycle of 12/12 h. The animals were fasted for 12 h prior to experiment, with food and water ad libitum. All the animal care and experimental protocols were performed according to the guidelines for the Care and Use of Laboratory Animals of Guangzhou Medical University. All animal experiments were approved by the Institutional Animal Care and Use Committee of Guangzhou Medical University (Acceptance number: S2021-099).

Fabrication of Hyaluronic Acid-Decorated RAPA Liposomes

Efficient solubilization is vital for achieving sufficient doses of hydrophobic RAPA in atherosclerotic lesions. We, therefore, fabricated liposomes by emulsion-solvent evaporation and sonication method. Briefly, the oil phase (OP) was composed of 15 mg RAPA, 120 mg phospholipid, dissolved in 2 mL dichloromethane (DCM). 20 mg cholesteryl sodium sulfate (CHOS) was ultrasonically dispersed in the aqueous phase (AP, 20 mL Tris-HCl) that contains 5% HA-DOPE

(phospholipid/HA-DOPE, w/w). Firstly, the OP was mixed with the AP and sonicated at 200 W for 2.5 min to form an emulsion, followed by a 45°C water bath to volatilize organic solvent. Then probe sonication (100 W, JY92IID ultrasonic processor, Ningbo Xinzhi Biotechnology Co., Ltd, China) was carried out for 3 min with ice-water bath. The unencapsulated RAPA were removed by filtration through a 0.22 μm cellulose nitrate membrane (Supplementary Material Section S.3. Determination of the trapping rate). The HA-decorated RAPA liposomes (HA-RL) were freeze-dried by a LGJ-10C freeze dryer (Beijing Sihuan Furuike Instrument Technology Development Co., Ltd, China) with 5% (w/v) lactose solution as the freeze-drying protective additive. Moreover, HA quantification was performed by the carbazole assay (Supplementary Material Section S.4. Hyaluronic Acid Quantification). Non-hyaluronic acid-decorated liposomes (RAPA-liposomes, RL), without the addition of HA-DOPE, were prepared by the same composition and method as the HA-RL. To trace the cell-uptake behavior of liposomes, the RAPA was replaced by 6-coumarin (HA-C6-LIP and C6-LIP) by the same procedure. DIR-loaded liposomes (HA-DIR-LIP and DIR-LIP) used for the near-infrared fluorescence imaging studies were also produced with a similar procedure (Supplementary Material Section S.5. Fabrication of Coumarin 6/DIR-loaded liposomes).

Physicochemical Characterization of RAPA Liposomes

Particle Size (nm), Zeta Potential (mV), and Morphologies

The mean particle size and ζ-potential of prepared liposomes were analyzed by dynamic laser light scattering (DLS) method using Malvern Zetasizer Nano ZS instrument at 25°C (ZEN3500, Nano ZS Instruments, Worcestershire, UK), repeating the measurement in triplicate. The polydispersity index (PDI) was also acquired by a cumulant analysis of the correlation function. The morphological investigation of liposomes was performed using transmission electron microscopy (TEM).

Fourier Transform Infra-Red Spectroscopy (FT-IR) and X-Ray Diffraction (XRD) Analysis

For FT-IR analysis, appropriate amounts of lyophilized RL and HA-RL powders were finely ground with potassium bromide (KBr) and thoroughly mixed. Subsequently, the mixtures were placed in the abrasive tool carefully and pressed into transparent flakes. A similar method was used to generate transparent flakes of RAPA and HA-DOPE samples. Then a FT-IR spectrophotometer was used to detect the infrared absorption spectrum of the resulting flakes in the spectral region of 400–4000 cm^{-1}, and the characteristic absorption peaks of the samples were analyzed. XRD analysis was also performed to investigate the crystallinity or amorphous nature of prepared liposomes. The diffractograms were recorded in the range of 2θ = 1–50° at a scanning rate of 2°/min.

Measurement of Entrapment Efficiency (EE%) of RAPA Liposomes

To measure EE% of RAPA liposomes, the RL and HA-RL were harvested by microporous membrane filtration (0.22 μm) and centrifugation (15,000 rpm, 15min, 4°C). 10 μL of the upper liposomes solution was added to 900 μL methanol for demulsification and centrifuged at 15,000 rpm for 15 min at 4°C. 10 μL of the supernatant was injected into the High Performance Liquid Chromatography (HPLC) apparatus for analysis. A C_{18} analytical column (Diamonsil® C18 Column, 4.6 mm×250 mm, 5 μm, Dikma Technologies Inc., China) was used for detection and the chosen wavelength was 278 nm. RAPA was well separated using an optimized mobile phase with methanol/acetonitrile/water(43/40/17, v/v/v) at a flow rate of 1.0 mL/min with a running time of 20 minutes (Supplementary Material Section S.6 HPLC methods for in vitro quantitation of RAPA). In addition, the results of methodological validation met the requirements for RAPA measurement (Figure 1S, Tables 1S–6S). The EE% was measured using the following equation:

$$\text{Entrapment efficiency } \% = \frac{\text{RAPA content in liposomes}}{\text{Theoretical RAPA content}} \times 100\%$$

Stability of Liposomes in vitro

The stability in vitro of RL and HA-RL was executed by determining the amount of drug or entrapment efficiency (EE%) and particle size. In particular, RAPA-loaded liposomes were added to Tris-HCl (pH 7.4) or 50% of the plasma (1:1, v/v) and the samples were incubated at 37°C with gentle shaking. At predetermined times (0, 1, 2, 4, 8, 12, and 24 h), the

particle size and drug amount were measured by method mentioned in Section 2.3. Meanwhile, the prepared liposomes were stored at 4°C and detected at 0, 7, 15, and 30 days to evaluate the storage stability.

Release Studies in vitro

A known quantity of RAPA liposomes lyophilized powder (RAPA concentration, 0.8 mg/mL) was reconstituted in 2 mL of fresh pH 7.5 PBS. The resulting dispersion was placed into a dialysis tube (MWCO of 12,000–14,000 Da), which was submerged into 100 mL release medium (0.01 M PBS with 0.5% SDS, pH 7.5, 6.5, 5.5). The beaker was vibrated continuously with 100 rotations/min at 37 ± 0.5 °C using an Orbital Shaker Bath. At predetermined time intervals (1, 1.5, 2, 3, 4, 6, 8, 10, 12, 24, 36, and 48 h), 1 mL of the dissolving medium was withdrawn and replaced with 1 mL of fresh release medium to maintain slot leakage conditions constantly. 1 mL DCM was added to each sample, and the extraction was vortexed thoroughly, then the supernatant (aqueous phase) was removed after standing and stratification. The residue was evaporated to dryness under a vacuum stream and reconstituted with 0.1 mL methanol prior to analysis. The amount of RAPA released into the dissolving medium was quantified by HPLC.

Cell Uptake and in vitro Assessment of the Lymphatic Targeting Property

To evaluate the lymphatic targeting of Hyaluronic acid-decorated liposomes, laser confocal scanning microscopy (LSCM) was used to observe the phagocytosis of liposomes. Lymphatic endothelial cells (LECS) were inoculated into 6-well plates (10×10^4 cells/well). After incubation for 24 h, the medium was replaced by fresh medium containing C6 solution, C6-LIP, HA-C6-LIP(6-coumarin [C6] = 5 μg/mL) and incubated for 1, 2, and 4 h. Notably, the LYVE-1 receptor blocking group was cultured in medium containing HA solution ([HA] = 0.4 mg/mL) for 4 hours before adding HA-C6-LIP to saturate receptor on the cell surface. Subsequently, the medium was removed and cells were fixed with 4% paraformaldehyde for 15–20 min, stained with DAPI (2.5 ug/mL) and washed thrice with sterile PBS. Laser confocal scanning microscopy imaging (LSCM, Nikon, Japan) was performed to observe the cell uptake, fluorescence distribution of DAPI and C6.

Bioanalytical LC–MS/MS Methods for RAPA

Plasma samples (100 μL) or tissue samples (200 μL, 20% w/w) were mixed with 500 μL of ice-cold methanol containing roxithromycin (100 ng/mL). After vortexing to sufficient extraction, the samples were centrifuged at 16,000 rpm for 15 min at 4°C. The supernatant was transferred into a new tube and evaporated under vacuum to dryness. The residue was reconstituted in 100 μL of methanol and centrifuged at 16,000 rpm for 15 min at 4°C. An aliquot of 10 μL of the supernatant was injected into the liquid chromatography-mass spectrometry (LC-MS/MS) apparatus for analysis (Supplementary Material Section S.7 Bioanalytical LC–MS/MS methods for RAPA). Meanwhile, the methodological evaluation of LC-MS/MS met the requirements of RAPA analysis in biological samples (Tables 7S–10S).

In vivo Pharmacokinetics

Eighteen SD rats were randomly divided into three groups. HA-RL, RL, and RAPA solution (RSM) were administered to the rats via tail intravenous injection at 2.0 mg/kg of RAPA. At predetermined time points (0.083, 0.1667, 0.25, 0.3333, 0.5, 1, 2, 4, 8, 12, and 24 h), the blood samples were collected from 18 animals and stored at −80°C until further analyzed by the methods assay mentioned in "Bioanalytical LC-MS/MS methods for RAPA" section. The pharmacokinetic parameters were calculated with the Drug and Statistics 2.0 (DAS2.0) software using a two-compartmental analysis model.

In vivo Evaluation on Lymphatic Targeting Efficiency and Biodistribution

To evaluate lymph node retention, HA-DIR-LIP, DIR-LIP, and free DIR solution were injected subcutaneously at 20 nmol of DIR (DIR, Near-infrared Fluorescent Dye). Mice were sacrificed and the lymph nodes (Inguinal LNs, Abdominal LNs, Axillary LNs, Cervical LNs, Popliteal LNs) were removed after 3 h. In vivo imaging system was used to observe fluorescence of lymph nodes and the radiation efficiency was also semi-quantitatively analyzed. Similar

procedures were followed to examine the biodistribution and targeting efficiency of HA-decorated drug delivery systems. The $LDLR^{-/-}$ mice were administrated via the tail vein at a single dose of 2.0 mg/kg. Mouse lungs, hearts, livers, spleens, kidneys, and lymph nodes were collected at 2, 4, 6, 8, and 12 h after injection. The tissues were accurately weighed and stored at −80°C to spare for analysis.

Experimental Anti-Atherosclerosis in $LDLR^{-/-}$ Mice

$LDLR^{-/-}$mice were given a normal diet containing 0.25 wt% cholesterol and 2 wt% lard for 3 months. The atherosclerosis model was established after 3 months of hyperlipid diet containing 1.5 wt% cholesterol and 15 wt% lard. Thirty-six mice were randomly divided into six groups (n = 6) and subjected to different treatments every 2 days for an additional 4 months: one model group received saline; one group treated with RSM via the tail vein at 2.0 mg/kg of RAPA; one group received RL by intravenous injection at 2.0 mg/kg of RAPA; three groups were treated with intravenous injection of HA-RL at 1.0 (low dose, HA-RL/L), 2.0 (medium dose, HA-RL/M), and 4.0 (high dose, HA-RL/H) mg/kg of RAPA, respectively; in addition, one control group was also included.

Analysis of Vascular Atherosclerotic Plaques in $LDLR^{-/-}$ As Model Mice

Blood was collected in heparinized anticoagulant tubes from the eyeballs of the mice after treatment for 2 months, and stored at −80°C to use for biochemical analysis after centrifugation at 3000 rpm/min for 10 min. The aortic vessels were obtained and opened longitudinally after the mice were sacrificed, the residual blood was washed out and they were stained with Sudan Red IV staining solution for 10 min. The atherosclerotic plaques were observed under a stereo microscope and photographed. An image analysis system was used to accurately delineate the contours of the whole vessel and the plaque, calculate the area of the whole vessel (A) and the plaque area (A_0), and obtain the ratio of plaque area to the whole vessel area (A_0/A). The aortic vessels was fixed in 10% formalin, then embedded in paraffin and sectioned. Atherosclerotic plaques were analyzed by hematoxylin-eosin (H&E) staining of 6-μm sections under an inverted fluorescence microscope (Nikon ECLIPSE Ti2).

Analysis of the Changes of Perivascular Lymphatic Vessels

"Whole mount immunofluorescence staining" method was used to observe the lymphatic distribution of blood vessels. In brief, vessels were immersed in ice-cold 4% PFA solution and fixed at 4°C. Subsequent tissue transparency, including dehydration and bleaching, was performed. After dehydration again and washing, the samples were blocked with 6% goat serum for 24 h and incubated with 3% goat serum containing primary antibody (LYVE-1 rabbit antibody) for 6 days, followed by incubation with secondary antibody diluent for 6 days. The samples were gradually dehydrated with methanol of different proportions (20%, 40%, 60%, 80%, 100%) for 1 h each. The samples were incubated in dibenzyl ether (DBE) until clarified and then stored at room temperature for fluorescence imaging by LSCM.

Lipid, Lipoprotein, and Inflammatory Cytokines Analysis

The levels of serum lipids including high-density lipoprotein (HDL), triglyceride (TG), total cholesterol (TCH), and low-density lipoprotein (LDL) were detected by a BK-200VET automatic biochemical analyzer (Olabo, China). Enzyme-linked immunosorbent assay kits were used to determine the levels of inflammatory cytokines, including MCP-1, TNF-α, IL-1β, MMP-3, and MMP-9.

Statistical Analysis

Data were expressed as the mean ± standard deviation (SD). Statistical analysis was executed using one-way analysis of variance (ANOVA) in GraphPad Prism 9.0 statistical software. P values less than 0.05 were considered significant.

Results and Discussion

Characterization of Liposomes and Stability Evaluation

Analysis showed that the RAPA-loaded liposomes formed a translucent liquid with a pale blue opalescence and presented an appropriate particle size (Figure 2A and B). The particle size was the most important factor affecting lymph node uptake, and the pertinent size ranges from 10–100 nm.[48,49] Herein, we reduced the particle sizes by ultrasonic and continuous extrusion, resulting in a uniform particle size distribution and smaller PDI, which could reduce the difference in uptake efficiency caused by heterogeneous particle size distribution. The mean particle sizes, PDI, zeta potentials and EE% of the liposomes are listed in Table 1. Particle sizes of liposomes with HA (size: 99.11±0.220 nm, PDI = 0.116 ±0.010) were slightly larger than those of liposomes without HA (size: 79.85±0.854 nm, PDI = 0.149±0.008), which indicates HA-DOPE had embedded into the lipid bilayer. Good drug encapsulation efficacy was required for the fabrication of a successful nano drug delivery system (NDDS), over 90% EE proved good loading ability of liposomes. The findings showed that EE of RL was 93.11±1.39% and that of HA-RL was 94.88±2.08%. The zeta potential of RL was −41.4±2.73 mV and that of HA-RL was −54.9±4.90, which revealed that HA successfully embedded into the phospholipid bilayer structure of liposomes. Besides, the results of HA quantification analysis showed that the binding rate of HA-DOPE to the phospholipid bilayer was as high as 93.37% (Table 11S). The zeta potentials of all liposomes are negative due to the existence of negatively charged (CHOS) and HA. The ζ-potential of liposomes higher than 30 mV was reported to make the liposomes repel each other, thereby avoiding particle aggregation and keeping the long-term stability of liposomes. The observation under transmission electron microscopy of the liposomes revealing their morphologically regular spherical nanostructures are shown in Figure 2C. Plasma stability was performed to simulate the in vivo hemocompatibility of liposomes. The adsorption of proteins on the liposomes could cause aggregation, and lead to an increase in particle size. The size and drug content showed no evident change during 24 h, indicating the good stability of the liposomes in plasma (Figure 2D). In addition, no visible size and drug content changes in two types of liposomes were observed after incubation for 24 h in PBS (pH 7.4). The results also showed no significant changes in size, and EE% after 30 days of storage at 4°C, implying an excellent storage stability of prepared liposomes (Figure 2E). These findings indicated the potential application and appropriateness for in vitro/vivo studies.

FT-IR and X-RD Analysis

The FT-IR spectrum of RAPA, HA-DOPE, RL, and HA-RL is shown in Figure 2F. The intense characteristic peaks of RAPA could be found at 3413.04 cm^{-1} (-OH stretching), 2822.82 cm^{-1}(C-H stretching), 1720.50cm^{-1}(C=C stretching), 1400.32cm^{-1} (combination of C-O and C=O, R-COO^{-} stretching), 1047.34 cm^{-1} and 613.36 cm^{-1} (C-O-C stretching). The infrared spectrum of HA-DOPE shows the characteristic peaks at 3417.86 cm^{-1} (-OH stretching), 2858.50 cm^{-1} (C-H stretching), 1738.82cm^{-1} (C=C stretching), 1620.20 cm^{-1}(N-H bending, amide II belt), 1410.92 cm^{-1} (combination of C-O and C=O, R-COO^{-} stretching), 1045.41 cm^{-1} and 610.47 cm^{-1} (C-O-C stretching), 1318.34 cm^{-1}(C-N, amide III belt). For RL and HA-RL, the characteristic peak of hydrogen bonding (3416.89 cm^{-1}, -OH stretching) enhanced absorption intensity, most of the characteristic peaks shared relatively similar absorption position as compared with RAPA and HA-DOPE standards. Therefore, these results confirmed that HA has been successfully modified on the surface of HA-RL. Furthermore, the amorphous HA-/RL complexes were revealed when X-ray diffraction (X-RD) was performed (Figure 2G).

In vitro Release

To comprehend the release mechanism of RAPA from HA-RL or RL, a dynamic dialysis method was executed to perform in vitro drug release studies. The in vitro drug release behavior was investigated with different environments at 37°C, simulating endosomal pH (5.5), tumor microenvironment pH (6.5), physiological condition (pH 7.4), respectively. As presented in Figure 2H, a significant RAPA release from RL or HA-RL was detected at pH 5.5, while relatively less release occurred at pH 6.5 and 7.4. Obviously, there is a sharp release in the first 2 h of the liposomes at pH 5.5, known as burst release, which resulted from the RAPA molecules being absorbed on the outer phospholipid layer of liposomes. Approximately 40% of the RAPA from liposomes was released during the first 2 h, implying the acid-triggered release of

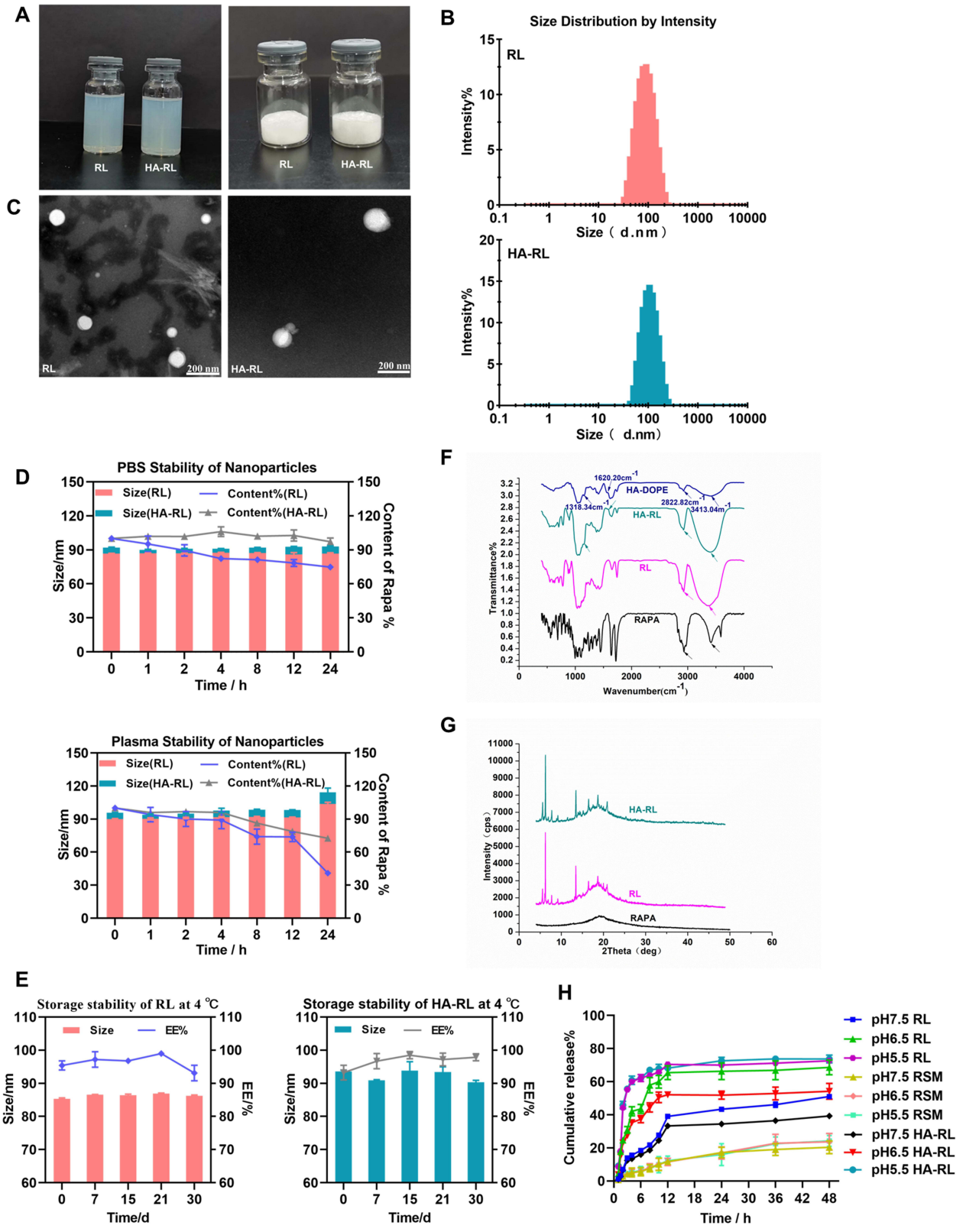

Figure 2 Characterization, stability evaluation and in vitro drug release studies of rapamycin liposomes. (**A**) Liposome samples. (**B**) Particle sizes. (**C**) TEM images of RL and HA-RL. (**D**) FTIR spectrum of HA-DOPE, RAPA, RL, and HA-RL. (**E**) X-RD pattern of HA-DOPE, RL, and HA-RL. (**F**) Stability of RL and HA-RL in PBS or 50% plasma at 37°C. (**G**) Stability of RL and HA-RL at 4°C after 30-days storage. (**H**) In vitro cumulative release profiles of RAPA from RSM, RL, and HA-RL (Mean ± SD, n = 3) under different physiological conditions (pH 7.4, 6.5, 5.5).

Table 1 Characteristics of Various LPs. Data are Presented as the Mean ± SD (n = 3)

Preparations	Size (nm)	PDI	Zeta Potential (mV)	EE (%)
RL	79.85±0.854	0.149±0.008	−41.4±2.73	93.11±1.39
HA-RL	99.11±0.220	0.116±0.010	−54.9±4.90	94.88±2.08

RL and HA-RL. The results also demonstrated that RL showed a biphasic release pattern with a slightly faster release rate, followed by a sustained releasing phase, without an initial burst at pH 6.5, 7.5. Release profile showed that about 40% of RAPA was released in the first 12 h followed by a sustained release of near 10% drug contents up to 48 h at pH 7.5, while this amount was around 60% at pH 6.5 in the first 12 h. Additionally, HA-RL also demonstrated a biphasic release pattern and the followed releasing phase exhibited a sustained release pattern. In particular, comparing the release profile of RL and HA-RL revealed that HA modification had prolonged the release of RAPA from liposomes. HA-RL exhibited a slower drug release and the total release amount of RAPA from HA-RL was less than that of RL after the same time, which was similar to a previous report that HA modification generates an additional barrier for drug diffusion, reducing the fluidity of the bilayer, as well as membrane permeability, resulting in the decreasing release rate of hydrophobic RAPA molecules. As for RSM, the release percentage of RAPA increased gradually at a slower release rate, with a cumulative release of about only 10% in the first 12 h followed by a more slow release and amount of near 20% cumulative release at 48 h. Moreover, the release behavior of RAPA from RSM was generally consistent at pH 7.5, 6.5, 5.5, with no difference, which might be due to RAPA being a lipophilic drug with low solubility, thus it was difficult to release into the medium.

In vivo Pharmacokinetic and Biodistribution Studies

The blood concentration-time profiles and pharmacokinetic parameters of RAPA after intravenous administration of different preparations are summarized in Figure 3A and Table 2. The blood concentration of rats rapidly reached the peak after tail vein administration, and it gradually decreased and tended to be relaxed thereafter. Meanwhile, the plasma concentration-time data were fitted with a weight of 1, and the pharmacokinetic models of RSM, RL, and HA-RL in rats conformed to the two-compartment model. As the results show, the clearance of RSM from blood circulation in rats was 2.1–4.5-fold faster than that of liposomal preparations. Consequently, all liposomal preparations were effective in enhancing systemic exposure and prolonging its blood circulation, and also boosted the efficiency of the lymphatic targeted delivery of RAPA. In addition, the AUC of RL and HA-RL was 1.8-fold and 4.6-fold higher (**P<0.01), respectively than that of RSM. Notably, the mean retention time (MRT) of HA-RL was significantly extended, which was 4.8-fold greater than that of RSM (*P<0.05). Furthermore, liposomal formulations also enhanced the elimination half-life ($t_{1/2\beta}$) of RAPA by 2.1–4.5-fold due to the decreased clearance, which effectively solves the problem of rapid metabolism of RAPA, thereby improving the bioavailability.

On the other hand, a non-invasive NIR fluorescence agent (DIR) was introduced to investigate the biodistribution of various formulations in $LDLR^{-/-}$ mice. As illustrated in Figure 3B, the retention of RL or HA-RL in LNs was dramatically higher than that in RSM, which may be because the natural lymphatic targeting of liposomes and the overexpression of LYVE-1 in lymphatic endothelial cells resulted in more internalization of HA-decorated liposomes via receptor mediated endocytosis. However, liposomal formulations also manifested a high fluorescence intensity in liver and spleen, and the fluorescence intensity and the amount of RAPA in liver and spleen in the HA-RL group were slightly higher than those in the RL group, which may be due to the inevitable phagocytosis of the nanoparticles by the reticuloendothelial system, also including the inherently high blood perfusion rate in liver, as other HA receptors are highly expressed in liver. Moreover, the retention of RAPA in lung was the highest of all tissues owing to pulmonary circulation after administration with different rapamycin preparations via tail vein injection. In addition, RAPA in the liver and spleen of the HA-RL and RL groups reached its maximum at 6 h, when there was less distribution in tissues other than lymph nodes, especially in lung (Figure 3C).

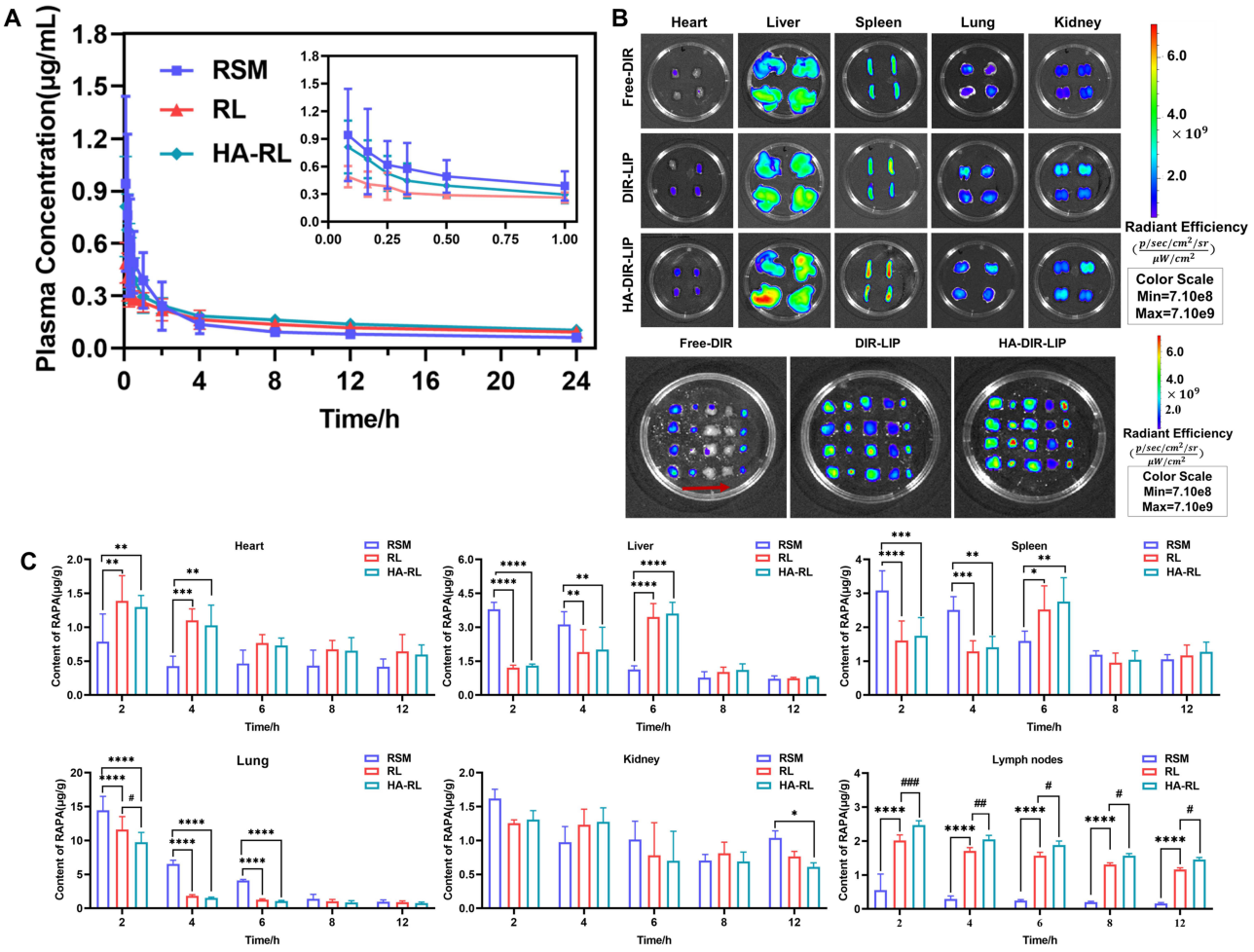

Figure 3 In vivo pharmacokinetic and biodistribution studies. (**A**) Plasma concentration-time curve after intravenous administration of RSM, RL, and HA-RL in rats (n = 6). (**B**) Fluorescence images after administration of Free-DIR, DIR-LIP, and HA-DIR-LIP in different tissues in LDLR$^{-/-}$ mice (n = 4) (Lymph nodes: Inguinal LNs, Abdominal LNs, Axillary LNs, Cervical LNs, Popliteal LNs). (**C**) RAPA concentration in different tissues after intravenous injection at the dose of 2.0 mg/kg in LDLR$^{-/-}$ mice (Mean ± SD, n = 4; RSM compared with RL or HA-RL, **P*<0.05, ***P*<0.01, ****P*<0.001, and *****P*<0.0001; RL compared with HA-RL, $^{\#}$*P*< 0.05, $^{\#\#}$*P*<0.01, and $^{\#\#\#\#}$*P*<0.001).

Lymphatic Targeting Ability in vitro and in vivo

Uptake of HA-LIP by lymphatic endothelial cells was evaluated by LSCM. As illustrated in Figure 4A, the amount of C6-loaded liposomes ingested into the cytoplasm of the LECs was higher than that of free-C6 after incubation at 37°C for 1, 2 and 4 h. The findings showed that the fluorescence intensity at 2 h and 4 h was stronger than that at 1 h, indicating

Table 2 Pharmacokinetic Parameters of RAPA After Intravenous Administration of RAPA in Different Formulations at the Dose of 2.0 mg/kg in Rats (mean ± SD, n = 6)

Parameters	Unit	RSM	RL	HA-RL
$t_{1/2\alpha}$	h	0.83±0.54	1.33±0.73	1.54±1.33
$t_{1/2\beta}$	h	15.73±5.67	33.52±15.72	70.74±50.80*
K_{10}	1/h	0.20±0.09	0.05±0.01	0.03±0.02
K_{12}	1/h	0.81±0.71	0.40±0.35	0.41±0.32
K_{21}	1/h	0.27±0.09	0.28±0.09	0.33±0.19
Cl	L/h/kg	0.12±0.02	0.06±0.02	0.09±0.13
$AUC_{0-\infty}$	mg/L*h	4.25±0.82	7.72±1.73	19.87±10.91**$^{\#}$
MRT	h	20.77±6.81	46.88±22.20	100.27±73.08*

Notes: RSM compared with HA-RL, **P*<0.05, ***P*<0.01; RL compared with HA-RL, $^{\#}$*P*<0.05.

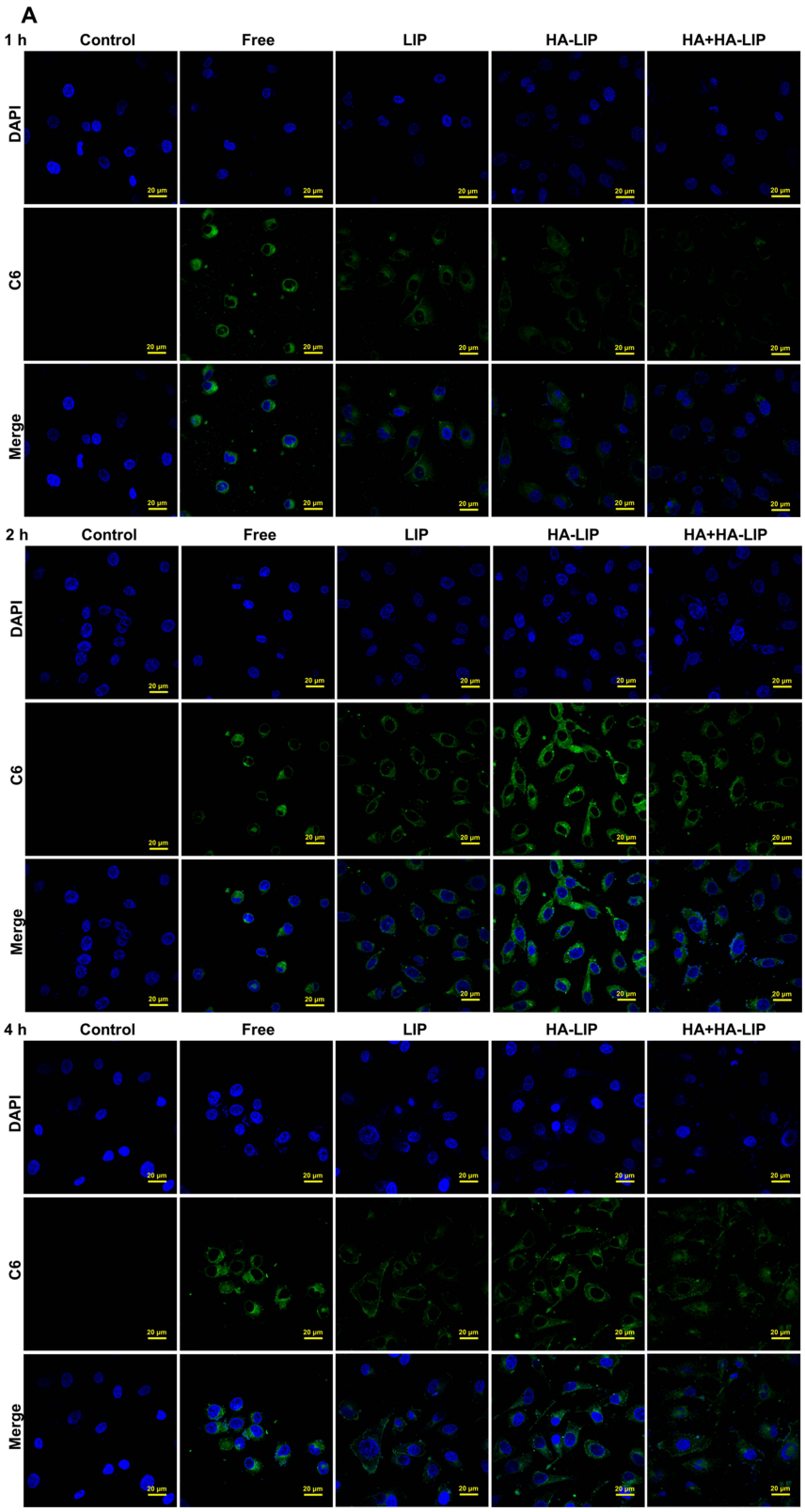

Figure 4 Continued.

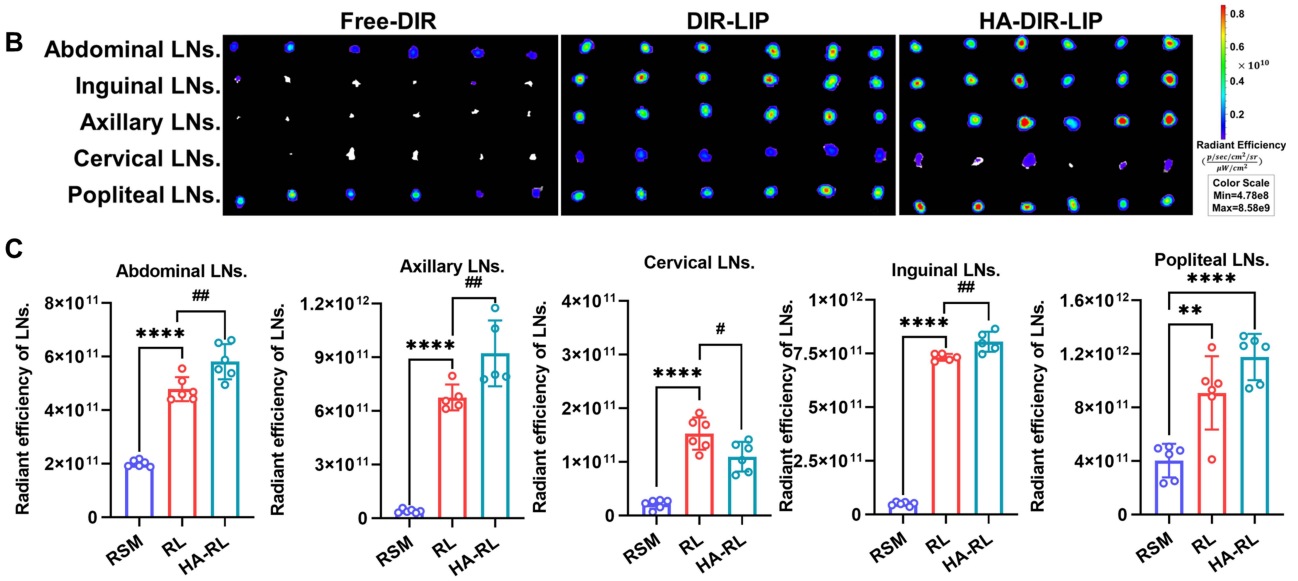

Figure 4 Evaluation of lymphatic targeting characteristics in vitro and in vivo. (**A**) LSCM fluorescence images of LECs after incubation with Free-C6, C6-LIP, and HA-C6-LIP for 1, 2, and 4 h ([C6] = 5 μg/mL). (**B**) Fluorescence images of excised LNs from $LDLR^{-/-}$mice (n = 6) by subcutaneous injection with 20 nmol Free-DIR, DIR-LIP, and HA-DIR-LIP (quantification was normalized according to the content of DIR). (**C**) Semi-quantitative radiant efficiency of the uptake of Free-DIR, DIR-LIP, and HA-DIR-LIP by the LNs at 3 hours after s.c administration (Mean ± SD; RSM compared with RL or HA-RL, ***P*<0.01, *****P*<0.0001; RL compared with HA-RL, $^{\#}P$< 0.05, $^{\#\#}P$<0.01).

that the uptake of liposomes by LECs increased with time, showing a time dependence, and the fluorescence intensity at 2 h was prominently stronger than that at 1 h. Notably, it can be clearly seen that most of the HA-C6-LIP are engulfed by cells, and tightly dispersed on the cell membrane, and some have even entered the cytoplasm. However, the fluorescence intensity decreased at 4 h, which we hypothesized was due to the exocytosis of the liposome nanoparticles as foreign material after being phagocytosed by LECs and reached saturation. Moreover, the fluorescence intensity of HA-C6-LIP is stronger than that of the C6-LIP without HA modification. This indicated that HA-C6-LIP acquired a high homologous targeting ability. Interestingly, the uptake of liposomes by the cells was reduced after the cells were pre-incubated with pure HA solution for 4 h, and the LYVE-1 receptor on the surface of LECs was blocked, which proved that the liposomes entered the cells via the LYVE-1 receptor mediated endocytosis. These findings indicated that HA-based liposomes have been successfully constructed, and this nanodelivery system has great potential for lymphatic targeting.

The liposomes with a particle size between 10 nm and 100 nm will effectively drain to lymph nodes. Encouraged by the excellent lymphatic targeting efficacy of HA-modified liposomes in vitro, the targeting efficacy in vivo was examined after s.c. administration. We assessed LN accumulation of free DIR, DIR-LIP, and HA-DIR-LIP using the whole fluorescence imaging system at the tissue level. As illustrated in Figure 4B and C, potentiated DIR fluorescence intensity can be seen in LNs (Inguinal LNs, Axillary LNs, Abdominal LNs, Cervical LNs, Popliteal LNs) after subcutaneously injected DIR-loaded liposomes. On the contrary, fluorescence signal can slightly be observed in LNs after s.c. injection of free DIR, which indicates that drug loaded into a nano carrier can effectively induce its flow to lymph nodes (*****P*<0.0001). Furthermore, HA-decorated liposomes enhanced the amount of liposomes accumulated in lymph nodes more through an active targeting effect. The findings proved that fluorescence intensity of HA-DIR-LIP was higher than that of the liposomes without HA decoration (***P*<0.01). What's more, the results of biodistribution were similar to those of lymph nodes fluorescence imaging; the amount of RAPA in liposomes, HA-decorated and not, was significantly higher than that found in RSM group when we detected the RAPA in lymph nodes (*****P*<0.0001). In addition, as demonstrated by the increase in fluorescence signal of lymph nodes in HA-RL group, we also found the amount of RAPA was observably higher than that in RL group (**P*<0.05). The above findings further confirmed that HA-RL can acquire lymphatic targeting more efficiently.

RAPA Effectively Attenuated the Growth of Atherosclerotic Plaques

RAPA has the potential effect of inducing the attenuation of atherosclerotic plaques, as well as the pleiotropic protective function of anti-atherosclerosis.[13] Thus, we examined whether RAPA inhibits the growth of atherosclerotic plaques,

treated LDLR$^{-/-}$ AS mouse model with drugs solution or entrapped in nanocarrier or HA-nanocarrier and investigated the effects of different formulations on the atherosclerotic plaques after treatment for 2 months. Representative images of vascular atherosclerosis plaques and H&E-stained sections of the aortic vessels are reported in Figure 5. As shown in Figure 5A, Sudan red IV staining showed the atherosclerotic plaques formation and the uneven thickness of the aortic wall. The area of atherosclerotic plaques in LDLR$^{-/-}$ mice given a hyperlipid diet for 3 months was much larger than that of the control group, which indicates the atherosclerosis model was successfully established. However, a significant reduction of atherosclerotic plaques can been found after the treatment with RAPA (P<0.01) (Figure 5B), these findings are also in agreement with the results of H&E-stained sections (Figure 5C). Moreover, the area of atherosclerotic plaques in HA-RL/L group (34.61±4.77 vs 45.10±3.59, P<0.05), HA-RL/M group (13.43±2.59 vs 45.10±3.59, P<0.0001), HA-RL/H group (17.38±2.11 vs 45.10±3.59, P<0.0001) were markedly smaller than that in RL group, respectively. Similarly, the total degree of vascular lumen stenosis in HA-RL groups was smaller than that in RL group and RSM group, respectively. Therefore, our findings showed that treatment with RAPA resulted in a conspicuous change in the atherosclerotic plaque area. Based on the experimental evidence that the hyaluronic acid-decorated rapamycin liposomes could obtain a more effective reduction in atherosclerotic plaque area, we hypothesized that the liposome modified with HA ligands may play a crucial role in the development of lymphatic targeting delivery systems.

To further verify our hypothesis that lymphatic targeted delivery of RAPA might be effective in reducing the proliferation of lymphatic vessels, a whole mount immunofluorescence staining test was used to analyze the perivascular lymphatic vessels (Figure 5D). The results of immunofluorescence imaging of the lymphatic vessels have shown that there were a large number of proliferating lymphatic vessels around the vessels in LDLR$^{-/-}$ AS mice, however, a significantly reduction of the lymphatic vessels was found after RAPA treatment. Interestingly, we noticed that administration with RAPA liposomes, actively targeted, caused a more conspicuous regression in lymphatic vessels, which further confirmed that the hyaluronic acid-modified liposomes could more effectively target the lymphatic vessels.

Effects of RAPA on Lipid, Lipoprotein, and Inflammatory Cytokines

Atherosclerosis is a chronic inflammatory disease, accompanied by the generation of a variety of vascular growth factors, cytokines, and chemokines, which also involves the metabolic abnormality of lipoprotein or lipoidosis.[38] To investigate the effect of RAPA on serum lipids and inflammatory cytokines, TCH, TG, LDL, HDL, and major cytokines including MCP-1, IL-1β, TNF-α, MMP-3, MMP-9 we detected. As shown in Figure 6A, a significant decrease of TCH, LDL, and TG in LDLR$^{-/-}$ AS model mice was found in either the RL group or the HA-RL groups, while HDL was distinctly increased after administration. Furthermore, the effect of increasing the level of HDL in HA-RL/M group was obviously stronger than that in RL group (3.25±0.17mmol/L vs 5.71±0.21mmol/L, n = 6, P<0.0001). These results suggested that RAPA can effectively ameliorate the metabolism of lipids, reducing the lipid deposition.

The above findings of a significant change in lipids metabolism prompted us to further investigate whether the treatment with RAPA induces inflammatory cytokine changes in serum (Figure 6B). Interleukin-1β (IL-1β) is a critical inflammatory factor mainly produced by activated mononuclear-macrophages,[50] which is considered to be a major regulator in atherosclerotic inflammatory response. The results showed that the levels of IL-1β in RAPA treatment groups (RL, HA-RL) was evidently lower than that in model group (P<0.0001). As a potent inflammatory factor, tumor necrosis factor α (TNF-α) is a key factor mediating various inflammatory reactions as well as an important factor in the formation of AS. Similar to what was observed in the changes of IL-1β, RAPA treatment groups (RL, HA-RL) had a significantly higher decrease in TNF-α levels than that of the model group (P<0.0001). To the best of our knowledge, foam cells formation is the basis and crux of atherosclerosis. Monocyte chemoattractant protein-I (MCP-1) is hardly expressed in normal vascular wall, but the expression of MCP-1 is increased in different stages of atherosclerosis, which mediates the whole process of monocyte from adhesion, migration to foam.[51] Therefore, it is important to examine whether the expression of MCP-1 in serum is affected by RAPA treatment, as the results revealed that the levels of MCP-1 were significantly decreased after administration, which strongly suggested that RAPA could inhibit the expression of MCP-1 and thus exerted an anti-atherosclerosis effect. In addition, the levels of MMP-3 in HA-RL groups were markedly lower than that in RL group (19.225±2.458 ng/mL vs. 31.617±1.381 ng/mL, n = 6, P<0.0001) and RSM group (19.225±2.458 ng/mL vs. 42.047±1.2.371 ng/mL, n = 6, P<0.0001), respectively. Nevertheless, although there was no conspicuous difference in HA-RL group compared with

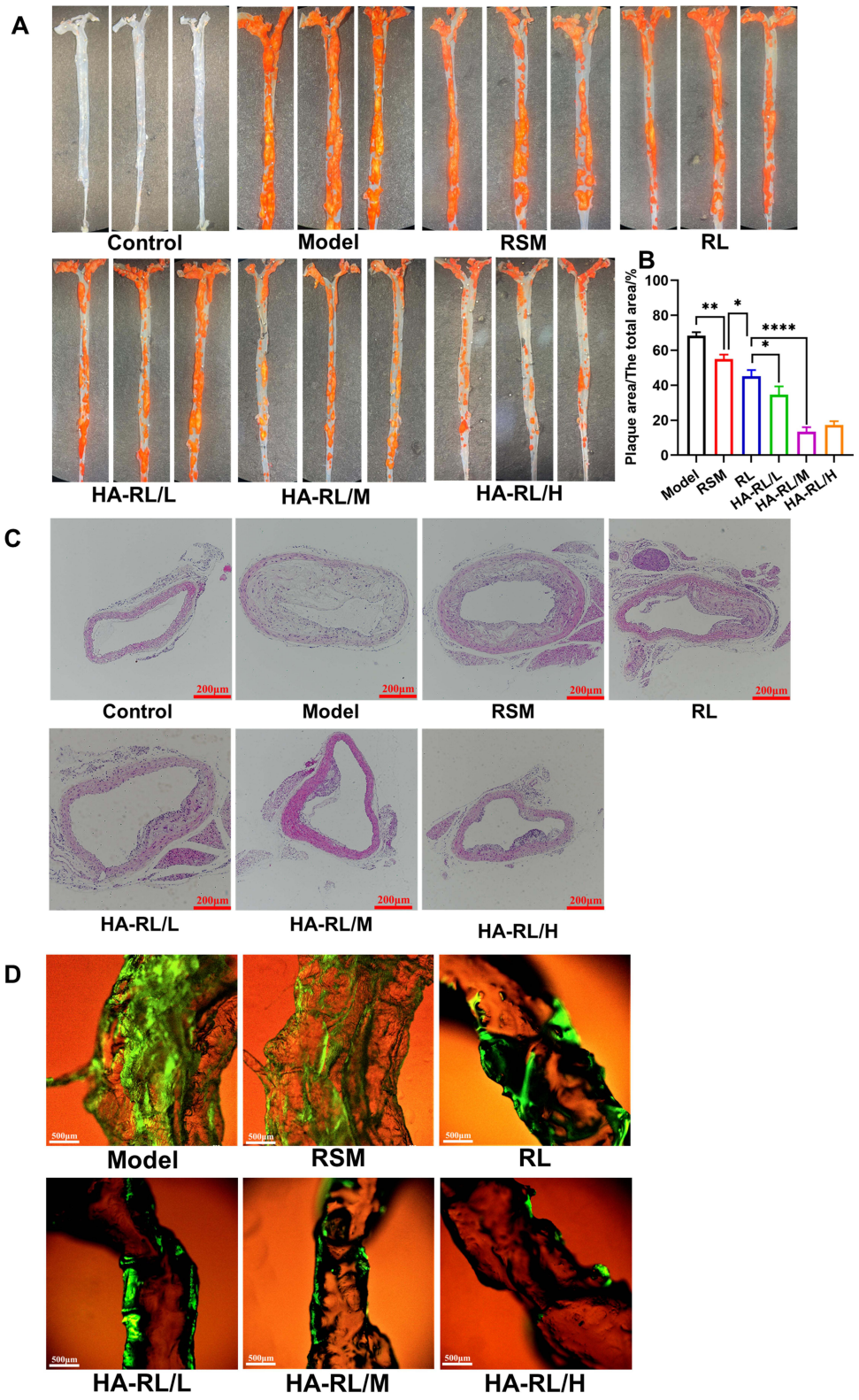

Figure 5 Effect of different RAPA preparations on the growth of atherosclerotic plaques in LDLR$^{-/-}$ mice (AS model). (**A**) Analysis of vascular atherosclerotic plaques after the LDLR$^{-/-}$ mice are administered different RAPA preparations for 2 months. (**B**) The plaque area (A_0) and whole vessel area ratio (A_1) was calculated, (A_0/A_1). (**C**) Analysis of the changes of perivascular lymphatic vessels. (**D**) H&E-stained images of aortic vessels were taken from all groups. Scale bar, 100 μm (Mean ± SEM; *P< 0.05, **P<0.01, and ****P<0.0001).

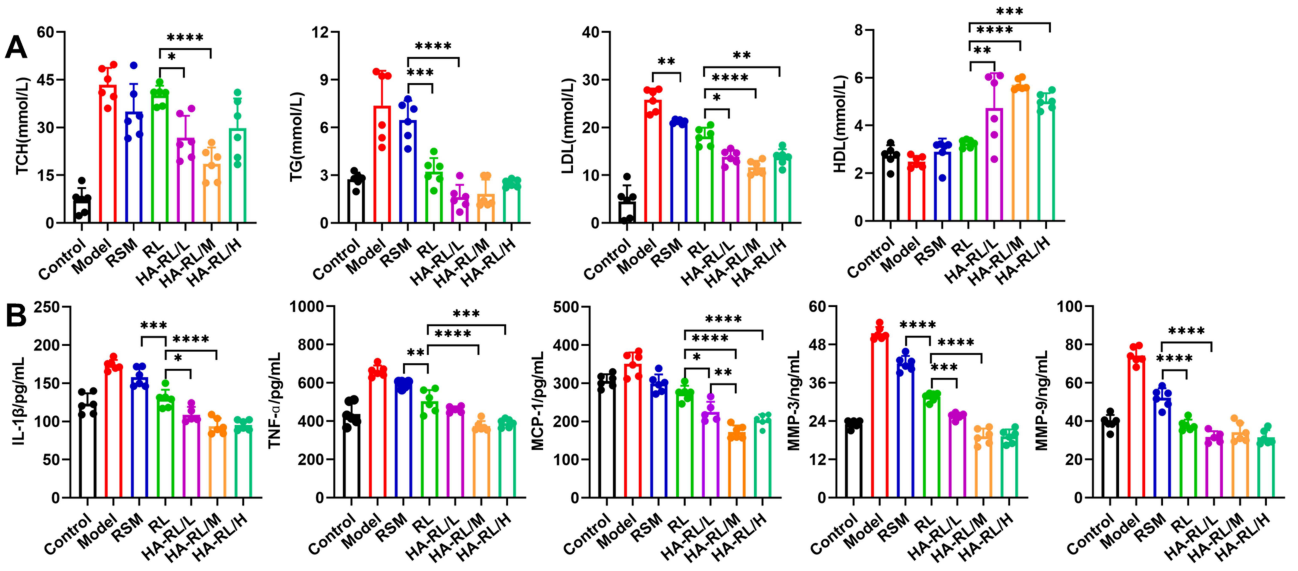

Figure 6 Effects of various RAPA preparations on lipid, lipoprotein, and inflammatory cytokines in LDLR$^{-/-}$ mice (AS model). After the LDLR$^{-/-}$ mice are administered various RAPA preparations for 2 months, the levels of HDL, LDL, TCH, and TG were measured (**A**), and the levels of MCP-1, TNF-α, IL-1β, MMP-3, and MMP-9 were examined by ELISA (**B**). (Mean ± SEM; *P < 0.05, **P < 0.01, ***P <0.001, and ****P<0.0001).

RL groups among the mice treated after 2 months, the relative descending level of MMP-9 in HA-RL groups was 0.11 times that of RL group. MMP-3 and MMP-9 are matrix metalloproteinases secreted by macrophages, neutrophils, and smooth muscle cells,[52] highly expressed in the vulnerable area of atherosclerotic plaques. They can degrade the basement membrane of the vascular wall and extracellular matrix, resulting in fibrin cap rupture and increase the instability of the plaque. The results proved that RAPA could reduce the expression of MMP-3/9, stabilize atherosclerotic plaques and induce plaques attenuation, thereby ameliorating the progression of atherosclerosis.

Conclusion

In this study, a novel pharmaceutical delivery system potentially useful for lymphatic-targeted drug delivery in the modulation of atherosclerosis has been developed. In detail, an advanced drug carrier for RAPA delivery was designed to efficiently disperse in an appropriate medium, resulting in a colloidal dispersed nanoparticle ready for in vivo delivery. For this purpose, a pertinet phospholipids material was introduced and surface-engineered liposomes were produced by emulsion-solvent evaporation method. During this process, hyaluronic acid, a site-specific ligand with a high affinity for the lymphatic endothelial cells LYVE-1 receptor, was also incorporated to acquire a lymphatic-targeted delivery system. In effect, the obtained nanoparticles have a particle size of less than 100 nm, propitious to lymphatic-targeted delivery, and entrapped large amounts of RAPA in amorphous form. Furthermore, the prepared liposomes were kept stable at 4°C, and the lyophilized powder could be reconstituted after dispersion in an appropriate medium with properties practically comparable to those of the initial liposomes, protecting the encapsulated drug from degradation and releasing it in a sustained manner.

Cytological studies on lymphatic endothelial cells have revealed that phagocytosis assay confirmed liposomes internalization, and in vitro studies were required to verify the efficiency of LYVE-1 targeting. Furthermore, the drug entrapped in the HA-decorated liposomes, actively targeted, has more efficacy in enhancing the cell uptake compared with the liposomes without HA, even the free drug. In addition, the results of the in vivo studies are momentous as it demonstrated that drugs embedded in nanocarriers could efficiently drain to LNs, and is more pronounced in HA-nano carriers. Furthermore, it is widely known that activation of lymphatic vessels is the crux to solve chronic inflammation and limit acute inflammation, and not only participates in the initiation and resolution of inflammation, but also plays an active role in cholesterol reversal. In this work, we provide significant and compelling evidence that the lymph-targeted liposomes could reduce the proliferation of lymphatic vessels, as well as reverse and stabilize the atherosclerotic plaques when MMP3/9 in serum was detected. Moreover, except for a slight decrease in TCH, it had little effect on TG while raising HDL. These results, taken together, manifested that RAPA liposomes, HA-decorated and not, had lymphatic

targeting characteristics and the potential to induce regression of atherosclerotic plaques, providing some inspiration for the development of an efficient NDDS in the treatment of atherosclerosis.

Acknowledgments

This work was supported by the National Natural Science Foundation of China (No. 81971742), the Natural Science Foundation of Guangdong Province (No. 2022A1515010199). The authors gratefully acknowledge The third Affiliated Hospital of Guangzhou Medical University for providing financial support.

Disclosure

The authors report no conflicts of interest in this work.

References

1. Virani Salim S, Alvaro A, Aparicio Hugo J, et al. Heart disease and stroke statistics—2021 update: a report from the American Heart Association. *Circulation*. 2021;143(8):e254–e743. doi:10.1161/CIR.0000000000000950
2. Siontis GC, Stefanini GG, Mavridis D, et al. Percutaneous coronary interventional strategies for treatment of in-stent restenosis: a network meta-analysis. *Lancet*. 2015;386(9994):655–664. doi:10.1016/S0140-6736(15)60657-2
3. Samidurai A, Kukreja RC, Das A. Emerging role of mTOR signaling-related miRNAs in cardiovascular diseases. *Oxid Med Cell Longev*. 2018;2018(614902):1–23. doi:10.1155/2018/6141902
4. Tousoulis D, Oikonomou E, Economou EK, Crea F, Kaski JC. Inflammatory cytokines in atherosclerosis: current therapeutic approaches. *Eur Heart J*. 2016;37(22):1723–1732. doi:10.1093/eurheartj/ehv759
5. Razani B, Feng C, Coleman T, et al. Autophagy links inflammasomes to atherosclerotic progression. *Cell Metab*. 2012;15(4):534–544. doi:10.1016/j.cmet.2012.02.011
6. Lavandero S, Chiong M, Rothermel BA, Hill JA. Autophagy in cardiovascular biology. *J Clin Invest*. 2015;125(1):55–64. doi:10.1172/JCI73943
7. Wynn TA, Chawla A, Pollard JW. Macrophage biology in development, homeostasis and disease. *Nature*. 2013;496(7446):445–455. doi:10.1038/nature12034
8. Matter MS, Decaens T, Andersen JB, Thorgeirsson SS. Targeting the mTOR pathway in hepatocellular carcinoma: current state and future trends. *J Hepatol*. 2014;60(4):855–865. doi:10.1016/j.jhep.2013.11.031
9. Liu Y, Yang F, Zou S, Qu L. Rapamycin: a bacteria-derived immunosuppressant that has anti-atherosclerotic effects and its clinical application. *Front Pharmacol*. 2019;9:1520.
10. Laplante M, Sabatini DM. MTOR signaling in growth control and disease. *Cell*. 2012;149(2):274–293. doi:10.1016/j.cell.2012.03.017
11. Wicki A, Witzigmann D, Balasubramanian V, et al. Nanomedicine in cancer therapy: challenges, opportunities, and clinical applications. *J Control Release*. 2015;200:138–157. doi:10.1016/j.jconrel.2014.12.030
12. Mahapatra AK, Murthy PN, Chandana S, et al. Progress with liposomal drug delivery systems: formulation to therapy. *Der Pharm Lett*. 2017;6(3):110–128.
13. Wang Y, Zhang K, Qin X, et al. Biomimetic nanotherapies: red blood cell based core-shell structured nanocomplexes for atherosclerosis management. *Adv Sci*. 2019;6(12):1900172. doi:10.1002/advs.201900172
14. Wang Y, Zhang K, Li T, et al. Macrophage membrane functionalized biomimetic nanoparticles for targeted anti-atherosclerosis applications. *Theranostics*. 2021;11(1):164–180. doi:10.7150/thno.47841
15. Boada C, Zinger A, Tsao C, et al. Rapamycin-loaded biomimetic nanoparticles reverse vascular inflammation. *Circ Res*. 2020;126(1):25–37. doi:10.1161/CIRCRESAHA.119.315185
16. Nordestgaard BG, Nicholls SJ, Langsted A, et al. Advances in lipid-lowering therapy through gene-silencing technologies. *Nat Rev Cardiol*. 2018;15(5):261–272. doi:10.1038/nrcardio.2018.3
17. Rosborough BR, Raïch-Regué D, Matta BM, et al. Murine dendritic cell rapamycin-resistant and rictor-independent mTOR controls IL-10, B7-H1, and regulatory T-cell induction. *Blood*. 2013;121(18):3619–3630. doi:10.1182/blood-2012-08-448290
18. Szwed A, Kim E, Jacinto E. Regulation and metabolic functions of mTORC1 and mTORC2. *Physiol Rev*. 2021;101(3):1371–1426. doi:10.1152/physrev.00026.2020
19. Liu Z, Fan Y, Zhang Z, et al. mTOR in the mechanisms of atherosclerosis and cardiovascular disease. *Discov Med*. 2021;31(164):129–140.
20. Sun JJ, Yin XW, Liu HH, et al. Rapamycin inhibits ox-LDL-induced inflammation in human endothelial cells in vitro by inhibiting the mTORC2/PKC/c-Fos pathway. *Acta Pharmacol Sin*. 2018;39(3):336–344. doi:10.1038/aps.2017.102
21. Gupta M, Ansell SM, Novak AJ, Kumar S, Kaufmann SH, Witzig TE. Inhibition of histone deacetylase overcomes rapamycin-mediated resistance in diffuse large B-cell lymphoma by inhibiting Akt signaling through mTORC2. *Blood*. 2009;114(14):2926–2935. doi:10.1182/blood-2009-05-220889
22. Dou Y, Guo J, Chen Y, et al. Sustained delivery by a cyclodextrin material-based nanocarrier potentiates antiatherosclerotic activity of rapamycin via selectively inhibiting mTORC1 in mice. *J Control Release*. 2016;235:48–62. doi:10.1016/j.jconrel.2016.05.049
23. Lameijer MA, Tang J, Nahrendorf M, Beelen RH, Mulder WJ. Monocytes and macrophages as nanomedicinal targets for improved diagnosis and treatment of disease. *Expert Rev Mol Diagn*. 2013;13(6):567–580. doi:10.1586/14737159.2013.819216
24. Cicha I, Chauvierre C, Texier I, et al. From design to the clinic: practical guidelines for translating cardiovascular nanomedicine. *Cardiovasc Res*. 2018;114(13):1714–1727. doi:10.1093/cvr/cvy219
25. Chen W, Schilperoort M, Cao Y, Shi J, Tabas I, Tao W. Macrophage-targeted nanomedicine for the diagnosis and treatment of atherosclerosis. *Nat Rev Cardiol*. 2022;19(4):228–249. doi:10.1038/s41569-021-00629-x
26. Vaidyanathan K, Gopalakrishnan S. Nanomedicine in the diagnosis and treatment of atherosclerosis-a systematic review. *Cardiovasc Hematol Disord Drug Targets*. 2017;17(2):119–131. doi:10.2174/1871529X17666170918142653

27. Hu B, Boakye-Yiadom KO, Yu W, et al. Nanomedicine approaches for advanced diagnosis and treatment of atherosclerosis and related ischemic diseases. *Adv Healthc Mater*. 2020;9(16):e2000336. doi:10.1002/adhm.202000336
28. Chan CKW, Zhang L, Cheng CK, et al. Recent advances in managing atherosclerosis via nanomedicine. *Small*. 2018;14(4):1702793. doi:10.1002/smll.201702793
29. Duivenvoorden R, Senders ML, van Leent MMT, et al. Nanoimmunotherapy to treat ischaemic heart disease. *Nat Rev Cardiol*. 2019;16(1):21–32. doi:10.1038/s41569-018-0073-1
30. Matsumoto Y, Nichols JW, Toh K, et al. Vascular bursts enhance permeability of tumour blood vessels and improve nanoparticle delivery. *Nat Nanotechnol*. 2016;11(6):533–538. doi:10.1038/nnano.2015.342
31. Tiantian Y, Wenji Z, Mingshuang S, et al. Study on intralymphatic-targeted hyaluronic acid-modified nanoliposome: influence of formulation factors on the lymphatic targeting. *Int J Pharm*. 2014;471(1–2):245–257. doi:10.1016/j.ijpharm.2014.05.027
32. Yan Z, Wang F, Wen Z, et al. LyP-1-conjugated PEGylated liposomes: a carrier system for targeted therapy of lymphatic metastatic tumor. *J Control Release*. 2012;157(1):118–125. doi:10.1016/j.jconrel.2011.07.034
33. Lei C, Liu XR, Chen QB, et al. Hyaluronic acid and albumin based nanoparticles for drug delivery. *J Control Release*. 2021;331:416–433. doi:10.1016/j.jconrel.2021.01.033
34. Tie S, Tan M. Current advances in multifunctional nanocarriers based on marine polysaccharides for colon delivery of food polyphenols. *J Agric Food Chem*. 2022;70(4):903–915. doi:10.1021/acs.jafc.1c05012
35. Yasin A, Ren Y, Li J, Sheng Y, Cao C, Zhang K. Advances in hyaluronic acid for biomedical applications. *Front Bioeng Biotechnol*. 2022;10:910290. doi:10.3389/fbioe.2022.910290
36. Libby P. Inflammation in atherosclerosis. *Arterioscler Thromb Vasc Biol*. 2012;32(9):2045–2051. doi:10.1161/ATVBAHA.108.179705
37. Anker S, Asselbergs FW, Brobert G, Vardas P, Grobbee DE, Cronin M. Big data in cardiovascular disease. *Eur Heart J*. 2017;38(24):1863–1865. doi:10.1093/eurheartj/ehx283
38. Yang X, Wang L, Zeng H, Dubey L, Zhou N, Pu J. Effects of simvastatin on NF-kappaB-DNA binding activity and monocyte chemoattractant protein-1 expression in a rabbit model of atherosclerosis. *J Huazhong Univ Sci Technol Med Sci*. 2006;26(2):194–198. doi:10.1007/BF02895814
39. Wiig H, Swartz MA. Interstitial fluid and lymph formation and transport: physiological regulation and roles in inflammation and cancer. *Physiol Rev*. 2012;92(3):1005–1060. doi:10.1152/physrev.00037.2011
40. Wolf D, Ley K. Immunity and inflammation in atherosclerosis. *Circ Res*. 2019;124(2):315–327. doi:10.1161/CIRCRESAHA.118.313591
41. Bennett MR, Sinha S, Owens GK. Vascular smooth muscle cells in atherosclerosis. *Circ Res*. 2016;118(4):692–702. doi:10.1161/CIRCRESAHA.115.306361
42. Aspelund A, Robciuc MR, Karaman S, Makinen T, Alitalo K. Lymphatic system in cardiovascular medicine. *Circ Res*. 2016;118(3):515–530. doi:10.1161/CIRCRESAHA.115.306544
43. Vengrenyuk Y, Nishi H, Long X, et al. Cholesterol loading reprograms the microRNA-143/145-myocardin axis to convert aortic smooth muscle cells to a dysfunctional macrophage-like phenotype. *Arterioscler Thromb Vasc Biol*. 2015;35(3):535–546. doi:10.1161/ATVBAHA.114.304029
44. Vieira JM, Norman S, Villa Del Campo C, et al. The cardiac lymphatic system stimulates resolution of inflammation following myocardial infarction. *J Clin Invest*. 2018;128(8):3402–3412. doi:10.1172/JCI97192
45. Jiang G, Park K, Kim J, et al. Hyaluronic acid-polyethyleneimine conjugate for target specific intracellular delivery of siRNA. *Biopolymers*. 2008;89(7):635–642. doi:10.1002/bip.20978
46. Dey A, Koli U, Dandekar P, Jain R. Investigating behavior of polymers in nanoparticles of chitosan oligosaccharides coated with hyaluronic acid. *Polymer*. 2016;93:44–52. doi:10.1016/j.polymer.2016.04.027
47. Jiang DH, Liang JR, Noble PW. Hyaluronan as an immune regulator in human diseases. *Physiol Rev*. 2011;91(1):221–264. doi:10.1152/physrev.00052.2009
48. Yang Z, Tian R, Wu J, et al. Impact of semiconducting perylene diimide nanoparticle size on lymph node mapping and cancer imaging. *ACS Nano*. 2017;11(4):4247–4255. doi:10.1021/acsnano.7b01261
49. Stylianopoulos T, Poh MZ, Insin N, et al. Diffusion of particles in the extracellular matrix: the effect of repulsive electrostatic interactions. *Biophys J*. 2010;99(5):1342–1349. doi:10.1016/j.bpj.2010.06.016
50. Lopez-Castejon G, Brough D. Understanding the mechanism of IL-1β secretion. *Cytokine Growth Factor Rev*. 2011;22(4):189–195. doi:10.1016/j.cytogfr.2011.10.001
51. Vinchi F, Porto G, Simmelbauer A, et al. Atherosclerosis is aggravated by iron overload and ameliorated by dietary and pharmacological iron restriction. *Eur Heart J*. 2020;41(28):2681–2695. doi:10.1093/eurheartj/ehz112
52. Carmona-Rivera C, Zhao W, Yalavarthi S, Kaplan MJ. Neutrophil extracellular traps induce endothelial dysfunction in systemic lupus erythematosus through the activation of matrix metalloproteinase-2. *Ann Rheum Dis*. 2015;74(7):1417–1424. doi:10.1136/annrheumdis-2013-204837